Constraints on Models for the Higgs Boson with Exotic Spin and Parity in $VH \to Vb\bar{b}$ Final States

V. M. Abazov,[31] B. Abbott,[67] B. S. Acharya,[25] M. Adams,[46] T. Adams,[44] J. P. Agnew,[41] G. D. Alexeev,[31] G. Alkhazov,[35] A. Alton,[56,a] A. Askew,[44] S. Atkins,[54] K. Augsten,[7] C. Avila,[5] F. Badaud,[10] L. Bagby,[45] B. Baldin,[45] D. V. Bandurin,[73] S. Banerjee,[25] E. Barberis,[55] P. Baringer,[53] J. F. Bartlett,[45] U. Bassler,[15] V. Bazterra,[46] A. Bean,[53] M. Begalli,[2] L. Bellantoni,[45] S. B. Beri,[23] G. Bernardi,[14] R. Bernhard,[19] I. Bertram,[39] M. Besançon,[15] R. Beuselinck,[40] P. C. Bhat,[45] S. Bhatia,[58] V. Bhatnagar,[23] G. Blazey,[47] S. Blessing,[44] K. Bloom,[59] A. Boehnlein,[45] D. Boline,[64] E. E. Boos,[33] G. Borissov,[39] M. Borysova,[38,l] A. Brandt,[70] O. Brandt,[20] R. Brock,[57] A. Bross,[45] D. Brown,[14] X. B. Bu,[45] M. Buehler,[45] V. Buescher,[21] V. Bunichev,[33] S. Burdin,[39,b] C. P. Buszello,[37] E. Camacho-Pérez,[28] B. C. K. Casey,[45] H. Castilla-Valdez,[28] S. Caughron,[57] S. Chakrabarti,[64] K. M. Chan,[51] A. Chandra,[72] E. Chapon,[15] G. Chen,[53] S. W. Cho,[27] S. Choi,[27] B. Choudhary,[24] S. Cihangir,[45] D. Claes,[59] J. Clutter,[53] M. Cooke,[45,k] W. E. Cooper,[45] M. Corcoran,[72] F. Couderc,[15] M.-C. Cousinou,[12] D. Cutts,[69] A. Das,[42] G. Davies,[40] S. J. de Jong,[29,30] E. De La Cruz-Burelo,[28] F. Déliot,[15] R. Demina,[63] D. Denisov,[45] S. P. Denisov,[34] S. Desai,[45] C. Deterre,[20,c] K. DeVaughan,[59] H. T. Diehl,[45] M. Diesburg,[45] P. F. Ding,[41] A. Dominguez,[59] A. Dubey,[24] L. V. Dudko,[33] A. Duperrin,[12] S. Dutt,[23] M. Eads,[47] D. Edmunds,[57] J. Ellison,[43] V. D. Elvira,[45] Y. Enari,[14] H. Evans,[49] V. N. Evdokimov,[34] A. Fauré,[15] L. Feng,[47] T. Ferbel,[63] F. Fiedler,[21] F. Filthaut,[29,30] W. Fisher,[57] H. E. Fisk,[45] M. Fortner,[47] H. Fox,[39] S. Fuess,[45] P. H. Garbincius,[45] A. Garcia-Bellido,[63] J. A. García-González,[28] V. Gavrilov,[32] W. Geng,[12,57] C. E. Gerber,[46] Y. Gershtein,[60] G. Ginther,[45,63] O. Gogota,[38] G. Golovanov,[31] P. D. Grannis,[64] S. Greder,[16] H. Greenlee,[45] G. Grenier,[17] Ph. Gris,[10] J.-F. Grivaz,[13] A. Grohsjean,[15,c] S. Grünendahl,[45] M. W. Grünewald,[26] T. Guillemin,[13] G. Gutierrez,[45] P. Gutierrez,[67] J. Haley,[68] L. Han,[4] K. Harder,[41] A. Harel,[63] J. M. Hauptman,[52] J. Hays,[40] T. Head,[41] T. Hebbeker,[18] D. Hedin,[47] H. Hegab,[68] A. P. Heinson,[43] U. Heintz,[69] C. Hensel,[1] I. Heredia-De La Cruz,[28,d] K. Herner,[45] G. Hesketh,[41,f] M. D. Hildreth,[51] R. Hirosky,[73] T. Hoang,[44] J. D. Hobbs,[64] B. Hoeneisen,[9] J. Hogan,[72] M. Hohlfeld,[21] J. L. Holzbauer,[58] I. Howley,[70] Z. Hubacek,[7,15] V. Hynek,[7] I. Iashvili,[62] Y. Ilchenko,[71] R. Illingworth,[45] A. S. Ito,[45] S. Jabeen,[45,m] M. Jaffré,[13] A. Jayasinghe,[67] M. S. Jeong,[27] R. Jesik,[40] P. Jiang,[4] K. Johns,[42] E. Johnson,[57] M. Johnson,[45] A. Jonckheere,[45] P. Jonsson,[40] J. Joshi,[43] A. W. Jung,[45] A. Juste,[36] E. Kajfasz,[12] D. Karmanov,[33] I. Katsanos,[59] R. Kehoe,[71] S. Kermiche,[12] N. Khalatyan,[45] A. Khanov,[68] A. Kharchilava,[62] Y. N. Kharzheev,[31] I. Kiselevich,[32] J. M. Kohli,[23] A. V. Kozelov,[34] J. Kraus,[58] A. Kumar,[62] A. Kupco,[8] T. Kurča,[17] V. A. Kuzmin,[33] S. Lammers,[49] P. Lebrun,[17] H. S. Lee,[27] S. W. Lee,[52] W. M. Lee,[45] X. Lei,[42] J. Lellouch,[14] D. Li,[14] H. Li,[73] L. Li,[43] Q. Z. Li,[45] J. K. Lim,[27] D. Lincoln,[45] J. Linnemann,[57] V. V. Lipaev,[34] R. Lipton,[45] H. Liu,[71] Y. Liu,[4] A. Lobodenko,[35] M. Lokajicek,[8] R. Lopes de Sa,[64] R. Luna-Garcia,[28,g] A. L. Lyon,[45] A. K. A. Maciel,[1] R. Madar,[19] R. Magaña-Villalba,[28] S. Malik,[59] V. L. Malyshev,[31] J. Mansour,[20] J. Martínez-Ortega,[28] R. McCarthy,[64] C. L. McGivern,[41] M. M. Meijer,[29,30] A. Melnitchouk,[45] D. Menezes,[47] P. G. Mercadante,[3] M. Merkin,[33] A. Meyer,[18] J. Meyer,[20,l] F. Miconi,[16] N. K. Mondal,[25] M. Mulhearn,[73] E. Nagy,[12] M. Narain,[69] R. Nayyar,[42] H. A. Neal,[56] J. P. Negret,[5] P. Neustroev,[35] H. T. Nguyen,[73] T. Nunnemann,[22] J. Orduna,[72] N. Osman,[12] J. Osta,[51] A. Pal,[70] N. Parashar,[50] V. Parihar,[69] S. K. Park,[27] R. Partridge,[69,e] N. Parua,[49] A. Patwa,[65,j] B. Penning,[45] M. Perfilov,[33] Y. Peters,[41] K. Petridis,[41] G. Petrillo,[63] P. Pétroff,[13] M.-A. Pleier,[65] V. M. Podstavkov,[45] A. V. Popov,[34] M. Prewitt,[72] D. Price,[41] N. Prokopenko,[34] J. Qian,[56] A. Quadt,[20] B. Quinn,[58] P. N. Ratoff,[39] I. Razumov,[34] I. Ripp-Baudot,[16] F. Rizatdinova,[68] M. Rominsky,[45] A. Ross,[39] C. Royon,[15] P. Rubinov,[45] R. Ruchti,[51] G. Sajot,[11] A. Sánchez-Hernández,[28] M. P. Sanders,[22] A. S. Santos,[1,h] G. Savage,[45] M. Savitskyi,[38] L. Sawyer,[54] T. Scanlon,[40] R. D. Schamberger,[64] Y. Scheglov,[35] H. Schellman,[48] C. Schwanenberger,[41] R. Schwienhorst,[57] J. Sekaric,[53] H. Severini,[67] E. Shabalina,[20] V. Shary,[15] S. Shaw,[57] A. A. Shchukin,[34] V. Simak,[7] P. Skubic,[67] P. Slattery,[63] D. Smirnov,[51] G. R. Snow,[59] J. Snow,[66] S. Snyder,[65] S. Söldner-Rembold,[41] L. Sonnenschein,[18] K. Soustruznik,[6] J. Stark,[11] D. A. Stoyanova,[34] M. Strauss,[67] L. Suter,[41] P. Svoisky,[67] M. Titov,[15] V. V. Tokmenin,[31] Y.-T. Tsai,[63] D. Tsybychev,[64] B. Tuchming,[15] C. Tully,[61] L. Uvarov,[35] S. Uvarov,[35] S. Uzunyan,[47] R. Van Kooten,[49] W. M. van Leeuwen,[29] N. Varelas,[46] E. W. Varnes,[42] I. A. Vasilyev,[34] A. Y. Verkheev,[31] L. S. Vertogradov,[31] M. Verzocchi,[45] M. Vesterinen,[41] D. Vilanova,[15] P. Vokac,[7] H. D. Wahl,[44] M. H. L. S. Wang,[45] J. Warchol,[51] G. Watts,[74] M. Wayne,[51] J. Weichert,[21] L. Welty-Rieger,[48] M. R. J. Williams,[49] G. W. Wilson,[53] M. Wobisch,[54] D. R. Wood,[55] T. R. Wyatt,[41] Y. Xie,[45] R. Yamada,[45] S. Yang,[4] T. Yasuda,[45] Y. A. Yatsunenko,[31] W. Ye,[64] Z. Ye,[45] H. Yin,[45] K. Yip,[65] S. W. Youn,[45] J. M. Yu,[56] J. Zennamo,[62] T. G. Zhao,[41] B. Zhou,[56] J. Zhu,[56] M. Zielinski,[63] D. Zieminska,[49] and L. Zivkovic[14]

(D0 Collaboration)

[1]LAFEX, Centro Brasileiro de Pesquisas Físicas, Rio de Janeiro, Brazil
[2]Universidade do Estado do Rio de Janeiro, Rio de Janeiro, Brazil
[3]Universidade Federal do ABC, Santo André, Brazil
[4]University of Science and Technology of China, Hefei, People's Republic of China
[5]Universidad de los Andes, Bogotá, Colombia
[6]Charles University, Faculty of Mathematics and Physics, Center for Particle Physics, Prague, Czech Republic
[7]Czech Technical University in Prague, Prague, Czech Republic
[8]Institute of Physics, Academy of Sciences of the Czech Republic, Prague, Czech Republic
[9]Universidad San Francisco de Quito, Quito, Ecuador
[10]LPC, Université Blaise Pascal, CNRS/IN2P3, Clermont, France
[11]LPSC, Université Joseph Fourier Grenoble 1, CNRS/IN2P3, Institut National Polytechnique de Grenoble, Grenoble, France
[12]CPPM, Aix-Marseille Université, CNRS/IN2P3, Marseille, France
[13]LAL, Université Paris-Sud, CNRS/IN2P3, Orsay, France
[14]LPNHE, Universités Paris VI and VII, CNRS/IN2P3, Paris, France
[15]CEA, Irfu, SPP, Saclay, France
[16]IPHC, Université de Strasbourg, CNRS/IN2P3, Strasbourg, France
[17]IPNL, Université Lyon 1, CNRS/IN2P3, Villeurbanne, France and Université de Lyon, Lyon, France
[18]III. Physikalisches Institut A, RWTH Aachen University, Aachen, Germany
[19]Physikalisches Institut, Universität Freiburg, Freiburg, Germany
[20]II. Physikalisches Institut, Georg-August-Universität Göttingen, Göttingen, Germany
[21]Institut für Physik, Universität Mainz, Mainz, Germany
[22]Ludwig-Maximilians-Universität München, München, Germany
[23]Panjab University, Chandigarh, India
[24]Delhi University, Delhi, India
[25]Tata Institute of Fundamental Research, Mumbai, India
[26]University College Dublin, Dublin, Ireland
[27]Korea Detector Laboratory, Korea University, Seoul, Korea
[28]CINVESTAV, Mexico City, Mexico
[29]Nikhef, Science Park, Amsterdam, the Netherlands
[30]Radboud University Nijmegen, Nijmegen, the Netherlands
[31]Joint Institute for Nuclear Research, Dubna, Russia
[32]Institute for Theoretical and Experimental Physics, Moscow, Russia
[33]Moscow State University, Moscow, Russia
[34]Institute for High Energy Physics, Protvino, Russia
[35]Petersburg Nuclear Physics Institute, St. Petersburg, Russia
[36]Institució Catalana de Recerca i Estudis Avançats (ICREA) and Institut de Física d'Altes Energies (IFAE), Barcelona, Spain
[37]Uppsala University, Uppsala, Sweden
[38]Taras Shevchenko National University of Kyiv, Kiev, Ukraine
[39]Lancaster University, Lancaster LA1 4YB, United Kingdom
[40]Imperial College London, London SW7 2AZ, United Kingdom
[41]The University of Manchester, Manchester M13 9PL, United Kingdom
[42]University of Arizona, Tucson, Arizona 85721, USA
[43]University of California Riverside, Riverside, California 92521, USA
[44]Florida State University, Tallahassee, Florida 32306, USA
[45]Fermi National Accelerator Laboratory, Batavia, Illinois 60510, USA
[46]University of Illinois at Chicago, Chicago, Illinois 60607, USA
[47]Northern Illinois University, DeKalb, Illinois 60115, USA
[48]Northwestern University, Evanston, Illinois 60208, USA
[49]Indiana University, Bloomington, Indiana 47405, USA
[50]Purdue University Calumet, Hammond, Indiana 46323, USA
[51]University of Notre Dame, Notre Dame, Indiana 46556, USA
[52]Iowa State University, Ames, Iowa 50011, USA
[53]University of Kansas, Lawrence, Kansas 66045, USA
[54]Louisiana Tech University, Ruston, Louisiana 71272, USA
[55]Northeastern University, Boston, Massachusetts 02115, USA
[56]University of Michigan, Ann Arbor, Michigan 48109, USA
[57]Michigan State University, East Lansing, Michigan 48824, USA
[58]University of Mississippi, University, Mississippi 38677, USA
[59]University of Nebraska, Lincoln, Nebraska 68588, USA
[60]Rutgers University, Piscataway, New Jersey 08855, USA

[61]*Princeton University, Princeton, New Jersey 08544, USA*
[62]*State University of New York, Buffalo, New York 14260, USA*
[63]*University of Rochester, Rochester, New York 14627, USA*
[64]*State University of New York, Stony Brook, New York 11794, USA*
[65]*Brookhaven National Laboratory, Upton, New York 11973, USA*
[66]*Langston University, Langston, Oklahoma 73050, USA*
[67]*University of Oklahoma, Norman, Oklahoma 73019, USA*
[68]*Oklahoma State University, Stillwater, Oklahoma 74078, USA*
[69]*Brown University, Providence, Rhode Island 02912, USA*
[70]*University of Texas, Arlington, Texas 76019, USA*
[71]*Southern Methodist University, Dallas, Texas 75275, USA*
[72]*Rice University, Houston, Texas 77005, USA*
[73]*University of Virginia, Charlottesville, Virginia 22904, USA*
[74]*University of Washington, Seattle, Washington 98195, USA*

We present constraints on models containing non-standard-model values for the spin J and parity P of the Higgs boson H in up to 9.7 fb^{-1} of $p\bar{p}$ collisions at $\sqrt{s} = 1.96$ TeV collected with the D0 detector at the Fermilab Tevatron Collider. These are the first studies of Higgs boson J^P with fermions in the final state. In the $ZH \to \ell\ell b\bar{b}$, $WH \to \ell\nu b\bar{b}$, and $ZH \to \nu\nu b\bar{b}$ final states, we compare the standard model (SM) Higgs boson prediction, $J^P = 0^+$, with two alternative hypotheses, $J^P = 0^-$ and $J^P = 2^+$. We use a likelihood ratio to quantify the degree to which our data are incompatible with non-SM J^P predictions for a range of possible production rates. Assuming that the production rate in the signal models considered is equal to the SM prediction, we reject the $J^P = 0^-$ and $J^P = 2^+$ hypotheses at the 97.6% CL and at the 99.0% CL, respectively. The expected exclusion sensitivity for a $J^P = 0^-$ ($J^P = 2^+$) state is at the 99.86% (99.94%) CL. Under the hypothesis that our data are the result of a combination of the SM-like Higgs boson and either a $J^P = 0^-$ or a $J^P = 2^+$ signal, we exclude a $J^P = 0^-$ fraction above 0.80 and a $J^P = 2^+$ fraction above 0.67 at the 95% CL. The expected exclusion covers $J^P = 0^-$ ($J^P = 2^+$) fractions above 0.54 (0.47).

After the discovery of a Higgs boson H at the CERN Large Hadron Collider (LHC) [1,2] in bosonic final states, and evidence for its decay to a pair of b quarks at the Tevatron experiments [3], and to pairs of fermions at the CMS experiment [4], it is important to determine the new particle's properties using all decay modes available. In particular, the spin and parity of the Higgs boson are important in determining the framework of the mass generation mechanism. The standard model (SM) predicts that the Higgs boson is a CP-even spin-0 particle ($J^P = 0^+$). If the Higgs boson is indeed a single boson, the observation of its decay to two photons at the LHC precludes spin 1 according to the Landau-Yang theorem [5,6]. Other J^P possibilities are possible. An admixture of $J^P = 0^+$ and $J^P = 0^-$ can arise in two-Higgs-doublet models [7,8] of type II such as found in supersymmetric models. A boson with tensor couplings ($J^P = 2^+$) can arise in models with extra dimensions [9]. The ATLAS and CMS Collaborations have examined the possibility that the H boson has $J^P = 0^-$ or $J^P = 2^+$ using its decays to $\gamma\gamma$, ZZ, and WW states [10–14]. The $J^P = 0^-$ hypothesis is excluded at the 97.8% and 99.95% CL by the ATLAS and CMS Collaborations, respectively, in the $H \to ZZ \to 4\ell$ decay mode. Likewise, the $J^P = 2^+$ hypothesis is excluded at the ≥ 99.9% CL by

the ATLAS Collaboration when combining all bosonic decay modes, and at the ≥ 97.7% CL by the CMS Collaboration in the $H \to ZZ \to 4\ell$ decay mode (depending on the production processes and the quark-mediated fraction of the production processes). However, the J^P character of Higgs bosons decaying to pairs of fermions, and in particular to $b\bar{b}$, has not yet been studied. In this Letter, we present tests of non-SM models describing the production of bosons with a mass of 125 GeV, $J^P = 0^-$ or $J^P = 2^+$, and decaying to $b\bar{b}$. We explore two scenarios for each of the hypotheses: (a) the new boson is a $J^P = 0^-$ ($J^P = 2^+$) particle and (b) the observed resonance is either a combination of these non-SM J^P states and a $J^P = 0^+$ state or distinct states with degenerate mass. In the latter case, we do not consider interference effects between states.

Unlike the LHC J^P measurements, our ability to distinguish different Higgs boson J^P assignments is not based primarily on the angular analysis of the Higgs boson decay products. It is instead based on the kinematic correlations between the vector boson V ($V = W, Z$) and the Higgs boson in VH associated production. Searches for associated VH production are sensitive to the different kinematics of the various J^P combinations in several observables,

especially the invariant mass of the VH system, due to the dominant p and d wave contributions to the $J^P = 0^-$ and $J^P = 2^+$ production processes [15–17]. The p and d wave contributions to the production cross sections near threshold vary as β^3 and β^5, respectively, whereas the s wave contribution for the SM Higgs boson varies as β, where β is the ratio of the Higgs boson momentum and energy.

To test compatibility of non-SM J^P models with data, we use the D0 studies of $ZH \to \ell\ell b\bar{b}$ [18], $WH \to \ell\nu b\bar{b}$ [19], and $ZH \to \nu\nu b\bar{b}$ [20] with no modifications to the event selections. Lepton flavors considered in the $WH \to \ell\nu b\bar{b}$ and $ZH \to \ell\ell b\bar{b}$ analyses include electrons and muons. Events with taus that decay to these leptons are considered as well, although their contribution is small. The D0 detector is described in Refs. [21–23].

We use 9.5– 9.7 fb^{-1} of integrated luminosity collected with the D0 detector satisfying relevant data-quality requirements in each of the three analyses. The SM background processes are either estimated from dedicated data samples (multijet backgrounds), or from Monte Carlo simulation. The $V + $ jets and $t\bar{t}$ processes are generated using ALPGEN [24], single top processes are generated using SINGLETOP [25], and diboson (VV) processes are generated using PYTHIA [26]. The SM Higgs boson processes are also generated using PYTHIA. The signal samples for the $J^P = 0^-$ and $J^P = 2^+$ hypotheses are generated using MADGRAPH 5 [27]. We have verified that $J^P = 0^+$ samples produced with MADGRAPH agree well with the SM PYTHIA prediction.

In the following, we denote a non-SM Higgs boson as X, reserving the label H for the SM $J^P = 0^+$ Higgs boson. MADGRAPH can simulate several non-SM models, as well as user-defined models. These new states are introduced via dimension-five Lagrangian operators [16]. The $J^P = 0^-$ samples are created using a model from the authors of Ref. [15]. The non-SM Lagrangian can be expressed as [16] $\mathcal{L}_{0^-} = (c_V^A/\Lambda)AF_{\mu\nu}\tilde{F}^{\mu\nu}$, where $F_{\mu\nu}$ is the field-strength tensor for the vector boson, A is the new boson field, c_V^A is a coupling term, and Λ is the scale at which new physics effects arise. The $J^P = 2^+$ signal samples are created using a Randall-Sundrum model, an extra-dimension model with a massive $J^P = 2^+$ particle that has gravitonlike couplings [28–31]. This model's Lagrangian can be expressed as $\mathcal{L}_{2^+} = (c_V^G/\Lambda)G^{\mu\nu}T_{\mu\nu}$, where $G^{\mu\nu}$ represents the $J^P = 2^+$ particle, c_V^G is a coupling term, $T_{\mu\nu}$ is the stress-energy tensor of the vector boson, and Λ is the effective Planck mass [9]. The mass of the non-SM Higgs-like particle X is set to 125 GeV, a value close to the mass measured by the LHC Collaborations [1,2] and also consistent with measurements at the Tevatron [3]. We study the decay of X to $b\bar{b}$ only. For our initial sample normalization we assume that the ratio μ of the product of the cross section and the branching fraction, $\sigma(VX) \times \mathcal{B}(X \to b\bar{b})$, to the SM prediction is $\mu = 1.0$ [32,33], and subsequently define exclusion regions as functions of μ. We generate samples using the

CTEQ6L1 parton distribution functions and use PYTHIA for parton showering and hadronization. The Monte Carlo samples are processed by the full D0 detector simulation. To reproduce the effect of multiple $p\bar{p}$ interactions in the same beam crossing, each simulated event is overlaid with an event from a sample of random beam crossings with the same instantaneous luminosity profile as the data. The events are then reconstructed with the same programs as the data.

All three analyses employ a b-tagging algorithm based on track impact parameters, secondary vertices, and event topology to select jets that are consistent with originating from a b quark [34,35].

The $ZH \to \ell\ell b\bar{b}$ analysis [18] selects events with two isolated charged leptons and at least two jets. A kinematic fit corrects the measured jet energies to their best fit values based on the constraints that the dilepton invariant mass should be consistent with the Z boson mass [36] and that the total transverse momentum of the leptons and jets should be consistent with zero. The event sample is further divided into orthogonal "single-tag" (ST) and "double-tag" (DT) channels according to the number of b-tagged jets. The SM Higgs boson search uses random forest [37] discriminants to provide distributions for the final statistical analysis. The first random forest is designed to discriminate against $t\bar{t}$ events and divides events into $t\bar{t}$-enriched and $t\bar{t}$-depleted ST and DT regions. In this study, only events in the $t\bar{t}$-depleted ST and DT regions are considered. These regions contain $\approx 94\%$ of the SM Higgs signal.

The $WH \to \ell\nu b\bar{b}$ analysis [19] selects events with one charged lepton, significant imbalance in the transverse energy ($\not{E}_T$), and two or three jets. This search is also sensitive to the $ZH \to \ell\ell b\bar{b}$ process when one of the charged leptons is not identified. Using the outputs of the b-tagging algorithm for all selected jets, events are divided into four orthogonal b-tagging categories, "one-tight-tag," "two-loose-tag," "two-medium-tag," and "two-tight-tag" (2TT). Looser b-tagging categories correspond to higher efficiencies for true b quarks and higher fake rates. Outputs from boosted decision trees (BDTs) [37], trained separately for each jet multiplicity and tagging category, serve as the final discriminants in the SM Higgs boson search.

The $ZH \to \nu\nu b\bar{b}$ analysis [20] selects events with large $\not{E}_T$ and exactly two jets. This search is also sensitive to the WH process when the charged lepton from the $W \to \ell\nu$ decay is not identified. A dedicated BDT is used to provide rejection of the large multijet background. Two orthogonal b-tagging channels, medium, and tight (TT), use the sum of the b-tagging discriminants of the two selected jets. BDT classifiers, trained separately for the different b-tagging categories, provide the final discriminants in the SM Higgs boson search.

These three analyses are among the inputs to the D0 SM Higgs boson search [38], yielding an excess above the SM background expectation that is consistent both in shape and in magnitude with a SM Higgs boson signal. The best fit to

data for the $H \to b\bar{b}$ decay channel for the product of the signal cross section and branching fraction is $\mu = 1.23^{+1.24}_{-1.17}$ for a mass of 125 GeV. When including data from both Tevatron experiments, the best fit to data yields $\mu = 1.59^{+0.69}_{-0.72}$ [39].

Discrimination between the J^P values of non-SM and SM hypotheses is achieved by using mass information of the VX system. For the $\ell\ell b\bar{b}$ final state we use the invariant mass of the two leptons and either the two highest b-tagged jets (DT) or the b-tagged jet and the highest p_T nontagged jet (ST) as the final discriminating variable. For the final states that have neutrinos, the discriminating variable is the transverse mass of the VX system which is defined as $M_T^2 = (E_T^V + E_T^X)^2 - (\vec{p}_T^V + \vec{p}_T^X)^2$ where the transverse momenta of the Z and W bosons are $\vec{p}_T^Z = \vec{E}_T$ and $\vec{p}_T^W = \vec{E}_T + \vec{p}_T^\ell$. For the $\ell\nu b\bar{b}$ final state, the two jets can either be one b-tagged jet (one-tight-tag) and the highest p_T nontagged jet, or the two b-tagged jets from any of the other three b-tagging categories: two-loose-tag, two-medium-tag, or 2TT.

To improve the discrimination between the non-SM signals and backgrounds in the $\ell\ell b\bar{b}$ and $\nu\nu b\bar{b}$ final states, we use the invariant mass of the dijet system M_{jj} to select two regions with different signal purities. Events with dijet masses in the range $100 \leq M_{jj} \leq 150$ GeV ($70 \leq M_{jj} < 150$ GeV) for $\ell\ell b\bar{b}$ ($\nu\nu b\bar{b}$) final states comprise the "high-purity" region (HP), while the remaining events are in the "low-purity region" (LP). As a result of the kinematic fit, the HP region for the $\ell\ell b\bar{b}$ final state is narrower than that for the $\nu\nu b\bar{b}$ final state, given the correspondingly narrower dijet mass peak. For the $\ell\nu b\bar{b}$ final state we use the final BDT output ($\mathcal{D}$) of the SM Higgs boson search [19]. Since events with $\mathcal{D} \leq 0$ provide negligible sensitivity to SM or non-SM signals, we do not consider them further. We

separate the remaining events into two categories with different signal purities. The LP category consists of events with $0 \leq \mathcal{D} \leq 0.5$, and the HP category of events with $\mathcal{D} > 0.5$.

Figure 1 illustrates the discriminating variables for the three analysis channels in the high-purity categories for the most sensitive b-tagging selections. Distributions for additional subchannels can be found in the Supplemental Material [40].

We perform the statistical analysis using a modified frequentist approach [38,41,42]. We use a negative log-likelihood ratio (LLR) as the test statistic for two hypotheses: the null hypothesis H_0 and the test hypothesis, H_1. This LLR is given by $\text{LLR} = -2\ln(L_{H_1}/L_{H_0})$, where L_{H_x} is the joint likelihood for hypothesis x evaluated over the number of bins in the final discriminating variable distribution in each channel. To decrease the effect of systematic uncertainties on the sensitivity, we fit the signals and backgrounds by maximizing the likelihood functions by allowing the systematic effects to vary within Gaussian constraints. This fit is performed separately for both the H_0 and H_1 hypotheses for the data and each pseudoexperiment.

We define CL_s as $\text{CL}_{H_1}/\text{CL}_{H_0}$ where CL_{H_x} for a given hypothesis H_x is $\text{CL}_{H_x} = P_{H_x}(\text{LLR} \geq \text{LLR}^{\text{obs}})$, and LLR^{obs} is the LLR value observed in the data. P_{H_x} is defined as the probability that the LLR falls beyond LLR^{obs} for the distribution of LLR populated by the H_x model. For example, if $\text{CL}_s \leq 0.05$ we exclude the H_1 hypothesis in favor of the H_0 hypothesis at $\geq 95\%$ CL.

Systematic uncertainties affecting both shape and rate are considered. The systematic uncertainties for each individual analysis are described in Refs. [18–20]. A summary of the major contributions follows. The largest contribution for all analyses is from the uncertainties on the
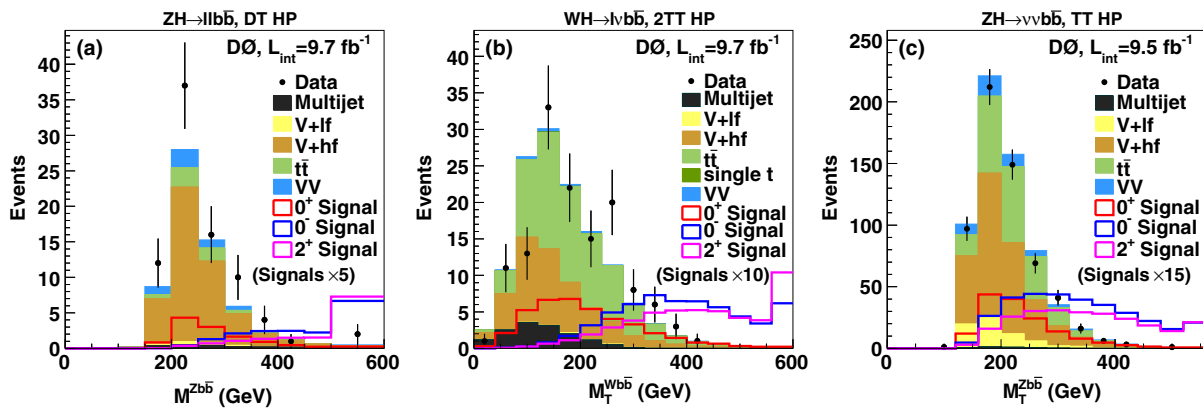

FIG. 1 (color online).   (a) Invariant mass of the $\ell\ell b\bar{b}$ system in the $ZH \to \ell\ell b\bar{b}$ high-purity double-tag (DT HP) channel, (b) transverse mass of the $\ell\nu b\bar{b}$ system in the $WH \to \ell\nu b\bar{b}$ high-purity two-tight-tag (2TT HP) channel, and (c) transverse mass of the $\nu\nu b\bar{b}$ system in the $ZH \to \nu\nu b\bar{b}$ high-purity tight-tag (TT HP) channel. The $J^P = 0^-$ and $J^P = 2^+$ samples are normalized to the product of the SM cross section and branching fraction multiplied by an additional factor. Heavy- and light-flavor quark jets are denoted by lf and hf, respectively. Overflow events are included in the highest mass bin. For all signals, a mass of 125 GeV for the H or X boson is assumed.
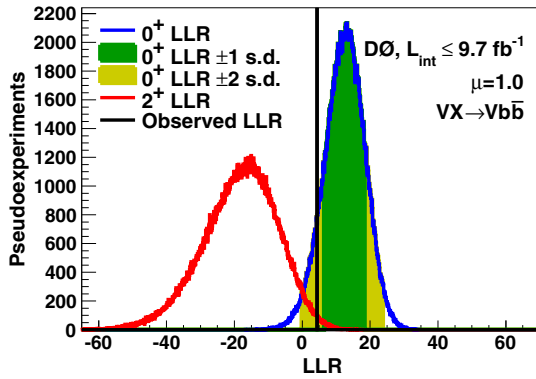
FIG. 2 (color online). LLR distributions comparing the $J^P = 0^+$ and the $J^P = 2^+$ hypotheses for the combination. The $J^P = 0^+$ and $J^P = 2^+$ samples are normalized to the product of the SM cross section and branching fraction. The vertical solid line represents the observed LLR value assuming $\mu = 1.0$, while the dark and light shaded areas represent the 1 and 2 standard deviations (s.d.) on the expectation from the null hypothesis H_0, respectively.

cross sections of the simulated V + heavy-flavor jets backgrounds which are 20%–30%. All other cross section uncertainties for simulated backgrounds are less than 10%. Since the multijet background is estimated from data, its uncertainty depends on the size of the data sample from which it is estimated, and ranges from 10% to 30%. All simulated samples for the $WH \to \ell\nu b\bar{b}$ and $ZH \to \nu\nu b\bar{b}$ analyses have an uncertainty of 6.1% from the integrated luminosity [43], whereas the simulated samples from the $ZH \to \ell\ell b\bar{b}$ analysis have uncertainties ranging from 0.7%–7% arising from the fitted normalization to the data [18]. All analyses take into account uncertainties on the jet energy scale, resolution, and jet identification efficiency for a combined uncertainty of ≈7%. The uncertainty on the b-tagging rate varies from 1%–10% depending on the number and quality of the tagged jets. The correlations between the three analyses are described in Ref. [38].

In this Letter, the H_0 hypothesis always contains SM background processes and the SM Higgs boson normalized to $\mu \times \sigma_{0^+}^{\mathrm{SM}}$. To test the non-SM cross section we assign the H_1 hypothesis as the sum of the $J^P = 0^-$ or $J^P = 2^+$ signal plus SM background processes, with no contribution from the SM Higgs boson. We calculate the CL_s values using signal cross sections expressed as $\mu \times \sigma_{0^+}^{\mathrm{SM}}$ and evaluate the expected values for each of these quantities by replacing $\mathrm{LLR}^{\mathrm{obs}}$ with $\mathrm{LLR}_{0^+}^{\mathrm{exp}}$, the median expectation for the $J^P = 0^+$ hypothesis only. Figure 2 illustrates the LLR distributions for the H_0 and $J^P = 2^+$ H_1 hypotheses, and the observed LLR value assuming $\mu = 1.0$, a production rate compatible with both Tevatron and LHC Higgs boson measurements. The similar plot for $J^P = 0^-$ is shown in the Supplemental Material [40]. We interpret $1 - \mathrm{CL}_s$ as the confidence level at which we exclude the non-SM hypothesis for the models considered in favor of

TABLE I. Expected and observed $1 - \mathrm{CL}_s$ values (converted to s.d. in parentheses) and signal fractions for $\mu = 1.0$ and $\mu = 1.23$ excluded at the 95% CL.

J^P	$1 - \mathrm{CL}_s$ (s.d.)		f_{J^P}	
$\mu = 1.0$	Expected	Observed	Expected	Observed
0^-	0.9986 (3.00)	0.976 (1.98)	> 0.54	> 0.80
2^+	0.9994 (3.22)	0.990 (2.34)	> 0.47	> 0.67
$\mu = 1.23$				
0^-	0.9998 (3.60)	0.995 (2.56)	> 0.45	> 0.67
2^+	0.9999 (3.86)	0.998 (2.91)	> 0.40	> 0.56

the SM prediction of $J^P = 0^+$ for the given value of μ. For $\mu = 1.0$ we exclude the $J^P = 0^-$ ($J^P = 2^+$) hypothesis at the 97.6% (99.0%) CL. The expected exclusions are at the 99.86% and 99.94% CL. Results, including those for $\mu = 1.23$, are given in Table I.

Tables detailing the CL_{H_x} values for each individual analysis channel and the combination can be found in the Supplemental Material [40]. We also obtain $1 - \mathrm{CL}_s$ over a range of SM and non-SM signal strengths. Figure 3 shows the expected and observed 95% CL exclusions as a function of the $J^P = 0^-$ ($J^P = 2^+$) and $J^P = 0^+$ signal strengths, which may differ between the SM and non-SM signals. In the tests shown in Fig. 3 the signal in the H_1 hypothesis is the $J^P = 0^-$ ($J^P = 2^+$) signal normalized to μ_{0^-} (μ_{2^+}) $\times \sigma_{0^+}^{\mathrm{SM}}$, and the signal in the H_0 hypothesis is the $J^P = 0^+$ signal normalized to $\mu_{0^+} \times \sigma_{0^+}^{\mathrm{SM}}$.

We also consider the possibility of a combination of J^P signals in our data (e.g., $J^P = 0^+$ and $J^P = 0^-$). These tests provide constraints on a number of theoretical models such as those containing pseudoscalar bosons in addition to a SM-like Higgs boson. For these studies we fix the sum of the two cross sections to a specific value of $\mu \times \sigma_{0^+}^{\mathrm{SM}}$ and vary the fractions $f_{0^-} = \sigma_{0^-}/(\sigma_{0^+} + \sigma_{0^-})$ or $f_{2^+} = \sigma_{2^+}/(\sigma_{0^+} + \sigma_{2^+})$ of non-SM signal and calculate the same
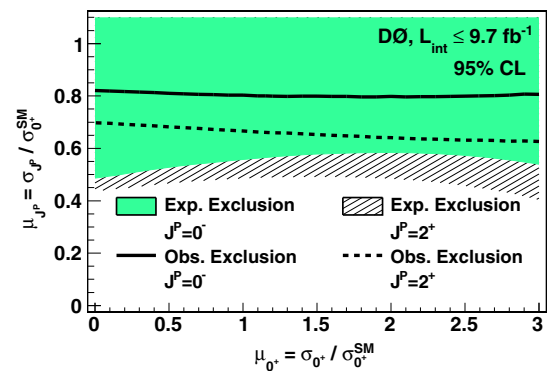

FIG. 3 (color online). The expected exclusion region (shaded area) and observed exclusion (solid line) as functions of the $J^P = 0^-$ and $J^P = 0^+$ signal strengths. The expected exclusion region (hatched area) and observed exclusion (dashed line) as functions of the $J^P = 2^+$ and $J^P = 0^+$ signal strengths.
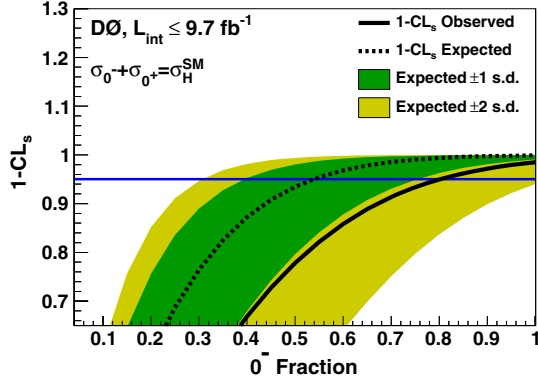
FIG. 4 (color online). $1 - \mathrm{CL}_s$ as a function of the $J^P = 0^-$ signal fraction assuming the product of the total cross section and branching ratio is equal to the SM prediction. The horizontal line corresponds to the 95% CL exclusion. The dark and light shaded regions represent the 1 and 2 s.d. fluctuations for the $J^P = 0^+$ hypothesis.

CL_s values as above as a function of f_{0^-} or f_{2^+}. To study f_{0^-}, we now modify H_1 to be the sum of the background, the $J^P = 0^-$ signal normalized to $\mu \times \sigma_{0^+}^{\mathrm{SM}} \times f_{0^-}$, and the $J^P = 0^+$ signal normalized to $\mu \times \sigma_{0^+}^{\mathrm{SM}} \times (1 - f_{0^-})$. H_0 remains as previously defined. We follow an identical prescription for $J^P = 2^+$. Figure 4 presents the value $1 - \mathrm{CL}_s$ as a function of the $J^P = 0^-$ signal fraction f_{0^-} for the case of $\mu = 1.0$, and the corresponding figure for the $J^P = 2^+$ hypothesis is available in the Supplemental Material [40]. For $\mu = 1.0$ we exclude a $J^P = 0^-$ ($J^P = 2^+$) signal fraction $f_{0^-} > 0.80$ ($f_{2^+} > 0.67$) at the 95% CL. The expected exclusions are $f_{0^-} > 0.54$ ($f_{2^+} > 0.47$). Limits on admixture fractions for other choices of μ are shown in the Supplemental Material [40].

In summary, we have performed tests of models with non-SM spin and parity assignments in Higgs boson production with a W or Z boson and decaying into $b\bar{b}$ pairs. We use the published analyses of the $WH \to \ell\nu b\bar{b}$, $ZH \to \ell\ell b\bar{b}$, and $ZH \to \nu\nu b\bar{b}$ final states with no modifications to the event selections. Sensitivity to non-SM J^P assignments in the two models considered here is enhanced via the separation of samples into high- and low-purity categories wherein the total mass or total transverse mass of the VX system provides powerful discrimination. Assuming a production rate compatible with both Tevatron and LHC Higgs boson measurements, our data strongly reject non-SM J^P predictions and agree with the SM $J^P = 0^+$ prediction. Under the assumption of two nearly degenerate bosons with different J^P values, we set upper limits on the fraction of non-SM signal in our data. This is the first exclusion of non-SM J^P parameter space in a fermionic decay channel of the Higgs boson.

[a]Visitor from Augustana College, Sioux Falls, SD, USA.
[b]Visitor from The University of Liverpool, Liverpool, UK.
[c]Visitor from DESY, Hamburg, Germany.
[d]Visitor from Universidad Michoacana de San Nicolas de Hidalgo, Morelia, Mexico.
[e]Visitor from SLAC, Menlo Park, CA, USA.
[f]Visitor from University College London, London, UK.
[g]Visitor from Centro de Investigacion en Computacion—IPN, Mexico City, Mexico.
[h]Visitor from Universidade Estadual Paulista, São Paulo, Brazil.
[i]Visitor from Karlsruher Institut für Technologie (KIT)—Steinbuch Centre for Computing (SCC), D-76128 Karlsruhe, Germany.
[j]Visitor from Office of Science, U.S. Department of Energy, Washington, DC 20585, USA.
[k]Visitor from American Association for the Advancement of Science, Washington, DC 20005, USA.
[l]Visitor from Kiev Institute for Nuclear Research, Kiev, Ukraine.
[m]Visitor from University of Maryland, College Park, Maryland 20742, USA.

[1] G. Aad *et al.* (ATLAS Collaboration), Phys. Lett. B **716**, 1 (2012).
[2] S. Chatrchyan *et al.* (CMS Collaboration), Phys. Lett. B **716**, 30 (2012).
[3] T. Aaltonen *et al.* (CDF and D0 Collaborations), Phys. Rev. Lett. **109**, 071804 (2012).
[4] S. Chatrchyan *et al.* (CMS Collaboration), Nat. Phys. **10**, 557 (2014).
[5] L. Landau, Dokl. Akad. Nauk Ser. Fiz. **60**, 207 (1948).
[6] C. N. Yang, Phys. Rev. **77**, 242 (1950).
[7] T. D. Lee, Phys. Rev. D **8**, 1226 (1973).
[8] E. Cerveró and J.-M. Gérard, Phys. Lett. B **712**, 255 (2012).
[9] R. Fok, C. Guimaraes, R. Lewis, and V. Sanz, J. High Energy Phys. 12 (2012) 062.

[10] S. Chatrchyan *et al.* (CMS Collaboration), Phys. Rev. Lett. **110**, 081803 (2013).

[11] G. Aad *et al.* (ATLAS Collaboration), Phys. Lett. B **726**, 120 (2013).

[12] S. Chatrchyan *et al.* (CMS Collaboration), J. High Energy Phys. 01 (2014) 096.

[13] S. Chatrchyan *et al.* (CMS Collaboration), Phys. Rev. D **89**, 092007 (2014).

[14] S. Chatrchyan *et al.* (CMS Collaboration), arXiv:1407.0558.

[15] J. Ellis, D. S. Hwang, V. Sanz, and T. You, J. High Energy Phys. 11 (2012) 134.

[16] J. Ellis, V. Sanz, and T. You, Eur. Phys. J. C **73**, 2507 (2013).

[17] D. Miller, S. Choi, B. Eberle, M. Mühlleitner, and P. Zerwas, Phys. Lett. B **505**, 149 (2001).

[18] V. M. Abazov *et al.* (D0 Collaboration), Phys. Rev. D **88**, 052010 (2013).

[19] V. M. Abazov *et al.* (D0 Collaboration), Phys. Rev. D **88**, 052008 (2013).

[20] V. M. Abazov *et al.* (D0 Collaboration), Phys. Lett. B **716**, 285 (2012).

[21] V. M. Abazov *et al.* (D0 Collaboration), Nucl. Instrum. Methods Phys. Res., Sect. A **565**, 463 (2006).

[22] M. Abolins *et al.*, Nucl. Instrum. Methods Phys. Res., Sect. A **584**, 75 (2008).

[23] R. Angstadt *et al.*, Nucl. Instrum. Methods Phys. Res., Sect. A **622**, 298 (2010).

[24] M. L. Mangano, M. Moretti, F. Piccinini, R. Pittau, and A. D. Polosa, J. High Energy Phys. 07 (2003) 001.

[25] E. E. Boos, V. E. Bunichev, L. V. Dudko, V. I. Savrin, and V. V. Sherstnev, Phys. At. Nucl. **69**, 1317 (2006).

[26] T. Sjöstrand, S. Mrenna, and P. Z. Skands, J. High Energy Phys. 05 (2006) 026.

[27] J. Alwall, M. Herquet, F. Maltoni, O. Mattelaer, and T. Stelzer, J. High Energy Phys. 06 (2011) 128. We use version 1.4.8.4.

[28] L. Randall and R. Sundrum, Phys. Rev. Lett. **83**, 3370 (1999).

[29] L. Randall and R. Sundrum, Phys. Rev. Lett. **83**, 4690 (1999).

[30] K. Hagiwara, J. Kanzaki, Q. Li, and K. Mawatari, Eur. Phys. J. C **56**, 435 (2008).

[31] P. Aquino, K. Hagiwara, Q. Li, and F. Maltoni, J. High Energy Phys. 06 (2011) 132.

[32] J. Baglio and A. Djouadi, J. High Energy Phys. 10 (2010) 064.

[33] O. Brein, R. V. Harlander, M. Wiesemann, and T. Zirke, Eur. Phys. J. C **72**, 1868 (2012).

[34] V. M. Abazov *et al.* (D0 Collaboration), Nucl. Instrum. Methods Phys. Res., Sect. A **763**, 290 (2014).

[35] V. M. Abazov *et al.* (D0 Collaboration), Nucl. Instrum. Methods Phys. Res., Sect. A **620**, 490 (2010).

[36] J. Beringer *et al.* (Particle Data Group), Phys. Rev. D **86**, 010001 (2012), and 2013 partial update for the 2014 edition.

[37] A. Hoecker *et al.*, *Proc. Sci.*, ACAT (2007) 040. We use version 4.1.0.

[38] V. M. Abazov *et al.* (D0 Collaboration), Phys. Rev. D **88**, 052011 (2013).

[39] T. Aaltonen *et al.* (CDF and D0 Collaborations), Phys. Rev. D **88**, 052014 (2013).

[40] See Supplemental Material at http://link.aps.org/supplemental/10.1103/PhysRevLett.113.161802 for additional figures and tables.

[41] A. L. Read, J. Phys. G **28**, 2693 (2002).

[42] W. Fisher, Report No. FERMILAB-TM-2386-E, 2007, http://lss.fnal.gov/archive/test-tm/2000/fermilab-tm-2386-e .pdf.

[43] T. Andeen *et al.*, Report No. FERMILAB-TM-2365, 2007, http://lss.fnal.gov/archive/test-tm/2000/fermilab-tm-2365 .pdf.